ELSEVIER

Chemical Physics 282 (2002) 361–370

Chemical Physics

www.elsevier.com/locate/chemphys

Rovibrational preexcitation in the photodesorption of CO from Cr_2O_3

S. Thiel[a,1], T. Klüner[a,*], D. Lemoine[b], H.-J. Freund[a]

[a] *Fritz-Haber Institut der Max-Planck-Gesellschaft, Faradayaweg 4-6, 14195 Berlin, Germany*

[b] *Laboratoire de Physique des Lasers, Atomes et Molécules, UMR CNRS, 8523 Centre d'Etudes et de Recherches Lasers et Applications, Université de Lille 1, Bâtiment P5, 59655 Villeneuve d'Ascq Cedex, France*

Received 22 April 2002

Abstract

The influence of rovibrational preexcitation in the $CO/Cr_2O_3(0\,0\,0\,1)$-system is studied theoretically using a three-dimensional quantum wave packet approach. We find that selectively excited hindered rotational levels of the adsorbate-substrate system influence the experimentally observed rotational alignment of the desorbing CO-molecule significantly. Pure vibrational preexcitation has less effect on the observables of interest. We predict only low surface temperature dependence of the rotational alignment and of the desorption yield. Our study is based on ab initio potential energy surfaces (PESs) for the electronic states involved and on a stochastic wave packet method.

PACS: 79.20.La; 71.15.Qe; 82.20.Kh

Keywords: Rotational alignment; Wave packet dynamics; Photodesorption

1. Introduction

The control of chemical reactivity in terms of manipulating product properties is one of the major goals of chemistry. It has been shown that carefully prepared laser pulses are a tuneable experimental parameter which drive chemical reactions towards specified directions [1]. In the field of photodesorption the experimental observables of interest are desorption cross-sections, velocity distributions or the phenomenon of rotational alignment of the desorbing species. Rotational alignment has been observed for CO molecules desorbing from a $Cr_2O_3(0\,0\,0\,1)$-surface in a quantum state resolved study [2]: Rotationally hot molecules prefer cartwheel motion (J vector perpendicular to the surface normal), in case of low rotational excitation the CO molecules desorb like helicopters (J vector parallel to the surface normal). Mechanistic understanding of this vector property was obtained recently [3,4]. The rotational alignment could be traced back to the

* Corresponding author. Fax: +49-30-84134101.
E-mail address: kluener@fhi-berlin.mpg.de (T. Klüner).
[1] Present address: Max-Planck-Institut für Kohlenforschung, Kaiser-Wilhelm-Platz 1, 45470 Mülheim an der Ruhr, Germany.

0301-0104/02/$ - see front matter
PII: S0301-0104(02)00770-X

azimuthal corrugations of the electronic potential energy surfaces involved in the photodesorption process.

One possible control parameter of such experimental observables is surface temperature. In one-dimensional studies, taking into account the center of mass distance of the molecule from the surface as the desorption coordinate, temperature has been shown to increase the desorption cross-sections of the exemplary systems NO/Pt [5] or CH_4/GaAs [6]. The role of thermal population of molecular vibrations within surface photochemistry was also studied using model potentials adapted to the system NO/Cr_2O_3(0 0 0 1). Direct comparison with experimental observations could be performed in that case [7]. Considering thermal effect means incoherent Boltzmann averaging of asymptotic observables. If only the desorption coordinate is accounted for, the discussion is limited to thermal preexcitation of the molecule–surface bond. It has been demonstrated that temperature effects on desorption cross-sections can be explained in terms of a quantum mechanical picture: After exciting the molecule–surface bond, the corresponding nuclear wavefunction has a larger extension than the lowest eigenstate. This accounts for more efficient desorption within the framework of the excitation–deexcitation cycle of a DIET (Desorption Induced by Electronic Transitions) process.

As another strategy of manipulating product properties vibrationally mediated photochemistry has been predicted theoretically for the system NH_3/Cu(1 1 1) in a two-dimensional model [8–10]. The umbrella mode of the adsorbed ammonia molecule is proposed to be excited in a first step with infrared pulses. UV irradiation then electronically excites the preexcited molecule. This strategy increases the desorption efficiency and allows for isotope specific desorption. In a 1D-study of NO/Pt(1 1 1) a positive effect of vibrational preexcitation on the desorption yield was found [11].

In the present study, we cover new aspects of control of a DIET process which arise from the high dimensional treatment as compared to previous studies. We treat the photodesorption of the exemplary CO/Cr_2O_3(0 0 0 1)-system in three dimensions and shed light on the microscopic desorption mechanism by taking into account molecular rotations in addition to the desorption degree of freedom. For the CO/Cr_2O_3(0 0 0 1)-system we will investigate the effects of selective excitation of the molecule–surface bond and of frustrated rotations of the adsorbed CO-molecule on experimental state resolved observables. We do not consider the step of selective excitation itself which requires the application of optimal control schemes [12,13].

2. 3D Potential energy surfaces and electronic ground state eigenfunctions

Based on a two state model, the photodesorption process is initiated by a sudden transition of an electronic ground (g) state eigenfunction $\Psi(0)$ to the electronically excited (e) state. This initial wave packet is propagated on the electronically excited state potential for a prespecified residence time t_n before deexcitation. The time evolution of the wave packet is calculated using the split operator propagator [14–16] and the action of the Hamiltonian on the wavefunction is carried out by a combined Fast Fourier/Gauss Legendre transform scheme [17–21]. The deexcited wave packet is then propagated on the ground state potential to a final time t of approximately 1.5 ps: $\Psi(t;t_n) = \mathrm{e}^{-\mathrm{i}\hat{H}_g(t-t_n)}\mathrm{e}^{-\mathrm{i}\hat{H}_e t_n}\Psi(0)$. At this time t, the observables $A(t,t_n)$ of interest are converged with respect to the total propagation time. This excitation–deexcitation cycle is repeated for several t_n. Finally, weighted lifetime averaging

$$A(t;\tau) = \sum_{n=1}^{n_{\max}} A(t;t_n)\exp\left(-\frac{t_n}{\tau}\right) \Bigg/ \sum_{n=1}^{n_{\max}} \exp\left(-\frac{t_n}{\tau}\right)$$

with respect to the resonance lifetime τ is performed [22].

Ab initio potential energy surfaces for both the electronic ground state (g) and an electronically excited state (e), corresponding to an internal $5\sigma \rightarrow 2\pi^*$ excitation of CO adsorbed on chromiumoxide have been calculated recently [23,24]. The degrees of freedom taken into account with respect to the CO motion above the surface where the

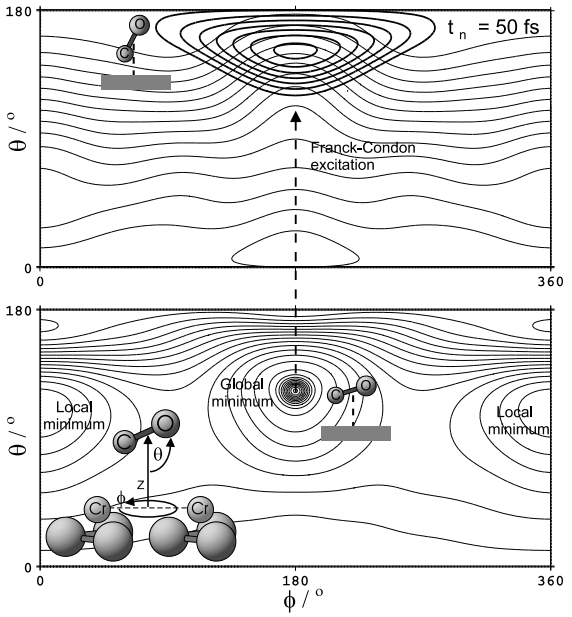

Fig. 1. 2D contour plots of the ab initio PES for the CO/Cr_2O_3(0 0 0 1)-system: θ–ϕ-dependences at ground state equilibrium value for the CO-distance ($Z = 4.5$ Bohr). Bottom: Electronic ground state with lowest rovibrational nuclear eigenstate. Top: Electronically excited $a^3\Pi$-state with snapshot of the wave packet after a time evolution of 50 fs. Inset: Cluster model used to represent the Cr_2O_3(0001)-surface.

desorption coordinate Z and the two angular coordinates θ and ϕ which describe the CO rotation as indicated in the inset of Fig. 1. This figure shows the angular topologies of the two electronic states involved as contour plots for the equilibrium distance of the CO molecule above the surface. As described previously [23], the CO molecule adsorbs strongly tilted with respect to the surface normal and in line with the Cr–Cr connection axis. Due to the excited state PES gradients along θ and ϕ, the molecule is both accelerated towards an upright adsorption geometry and is kicked out of its in line configuration with respect to the Cr–Cr axis after laser irradiation.

The nuclear eigenfunctions of the electronic ground state PES were calculated by propagation in imaginary time [25]. In Fig. 2, we show the energy level diagram and contour plots of some corresponding nuclear wavefunctions. Excitation of the molecule–surface vibration is visible by an increasing number of Z-nodes in the Z–θ-distributions on the right. Due to the corrugation of the electronic ground state PES with respect to θ and ϕ, the CO rotation on the surface is hindered. The spacing of the rotational energy levels is large as compared to the molecule–surface vibrational levels and as compared to the situation in gas phase. This means that rotational excitation needs more energy than excitation of molecule–surface vibration. The two nearly degenerate levels with nodes in θ and ϕ (on the top right of Fig. 2) correspond to this hindered rotation. At an energy of −0.004014 a.u., a rovibrational level occurs in a local minimum of the electronic ground state PES. This local minimum corresponds to the situation, in which the CO molecule is rotated by 180° with respect to ϕ, reaching an even more tilted adsorption geometry which exhibits less binding energy. The energies and populations

$$p_i = \exp\left(-\frac{E_i}{kT}\right) \Big/ \sum_i \exp\left(-\frac{E_i}{kT}\right)$$

at the experimental temperature of $T = 100$ K and, for comparison, at $T = 500$ K are collected in Table 1.

3. Excited state dynamics

In a first step of our calculations, an electronic ground state eigenfunction is placed on the electronically excited state and propagated for a residence lifetime t_n. In Fig. 3 we show expectation values for θ and Z as a function of the excited state residence time t_n. The eigenstates of the electronic ground state PES are transferred to the electronically excited state PES separately. The motion of the vertically excited wave packet is followed without deexciting it onto the electronic ground state PES. Independent of rotational or vibrational preexcitation of the initial state, the expectation values for θ display an oscillatory behaviour corresponding to a hindered rotation of the CO-molecule with respect to the surface normal after laser excitation. The amplitude mainly depends on the nodal structure of the initial state with respect to the angular coordinates θ and ϕ. The different curves presented for a specific number of nodes in the angular coordinates correspond to different

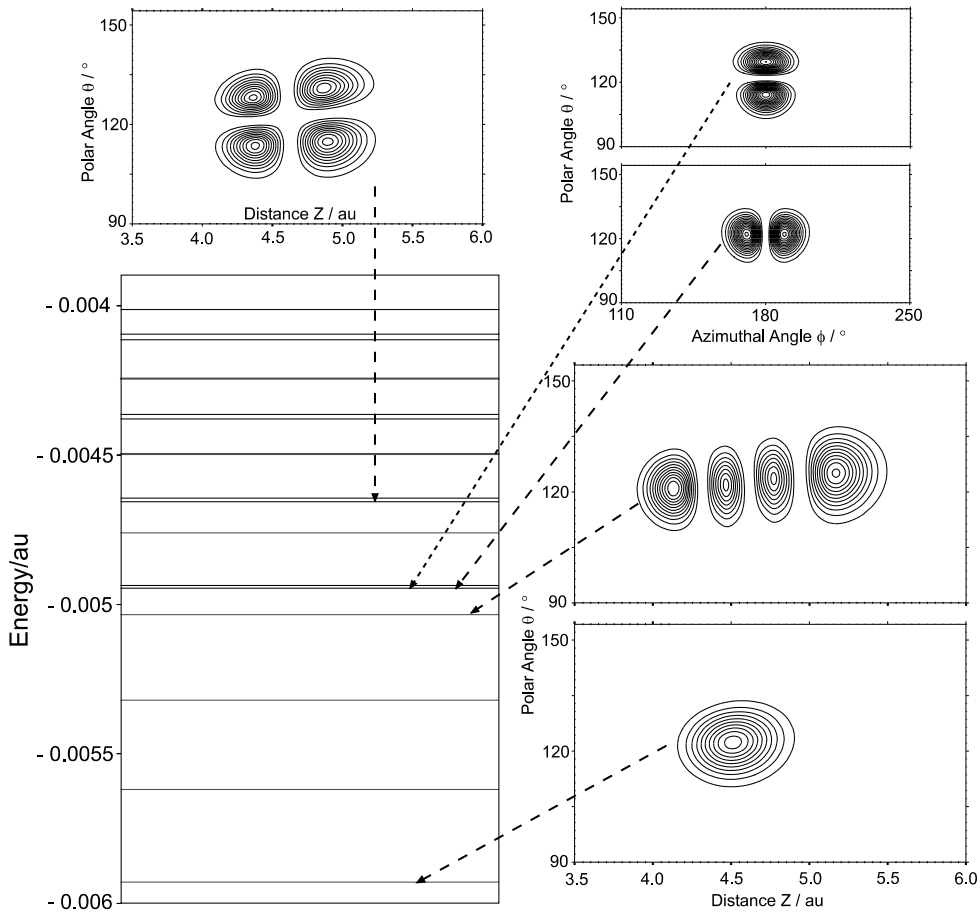

Fig. 2. Energy level diagram and contour plots of some chosen eigenfunctions of 3D electronic ground state PES. For the energies and populations of the corresponding levels at two different temperatures see Table 1.

numbers of nodes along the desorption coordinate Z. For a given initial θ–ϕ excitation the amplitude of the oscillation does not change significantly with increasing excitation of the molecule–surface bond. As it is visible in Fig. 3(right) not much motion in the molecule surface bond itself is excited by the laser irradiation. Independent of the prepared state, the expectation value for the desorption coordinate Z oscillates with a small amplitude of only about 0.1 a.u. Distinguishing between the well known one-dimensional MGR- and Antoniewicz-models [26–28] seems not reasonable, since the molecule is first repelled from the surface before being forced backwards to smaller distances due to the Z–θ topolgy of the electronically excited state. Interestingly, the hindered rotational level, which is located in the local minimum of the electronic ground state PES, behaves differently: In this configuration, the CO molecule is accelerated towards the surface after laser excitation in the sense of an Antoniewicz-mechanism [26].

4. Influence of initial state

4.1. Desorption probability

After deexcitation at t_n, the evolution of the wave packet on the ground state potential is continued until the desorption event is complete at the final time t. The desorption probability P_{des} is

Table 1
Energy levels of 3D electronic ground state PES

Energy (a.u.)	Population (100 K)	Population (500 K)	nodes: Z–θ–ϕ
−0.0059294697	0.5648	0.1212	0–0–0
−0.0056191213	0.2118	0.0996	1–0–0
−0.0053209454	0.0826	0.0825	2–0–0
−0.0050346787	0.0334	0.0689	3–0–0
−0.0049455855	0.0252	0.0651	0–1–0
−0.0049367704	0.0245	0.0647	0–0–1
−0.0047600396	0.0140	0.0579	4–0–0
−0.0046563247	0.0101	0.0542	1–1–0
−0.0046447196	0.0097	0.0538	1–0–1
−0.0044967456	0.0061	0.0490	5–0–0
−0.0043797205	0.0042	0.0455	2–1–0
−0.0043649611	0.0040	0.0451	2–0–1
−0.0042445158	0.0028	0.0418	6–0–0
−0.0041154449	0.0018	0.0385	3–1–0
−0.0040972341	0.0017	0.0381	3–0–1
−0.0040141251	0.0013	0.0361	0–2–0
−0.0040944778	0.0017	0.0380	0–0–0

computed from the square norm of the part of the wave packet which has reached the asymptotic zone of the electronic ground state potential. This desorbed part of the wavefunction is separated by a smooth transfer function as described elsewhere [29]. Before averaging over residence lifetimes it is instructive to focus on the dependence of single desorption events, in order to gain more detailed insight into the microscopic picture of the process. Fig. 4 shows the desorption probability as a function of the excited state residence lifetime t_n for several initial states.

From Fig. 4, we can deduce that the angular degrees of freedom (θ and ϕ) are very important for the microscopic understanding of the desorption process. Selective excitation of hindered rotational levels with nodes either in the polar angle θ or the azimuthal angle ϕ has more significant consequences on the asymptotic desorption probability than selective excitation of the molecule–surface vibrational mode. Molecule–surface vibrations do not much influence the desorption probability for a given initial θ–ϕ preexcited state. Excitation of the azimuthal rotational mode enhances the desorption probability considerably. The microscopic reason is the large spatial extension of these states as compared to the rovibrational ground state. The electronic ground state potential becomes repulsive immediately when the CO-molecule is shifted out of its Cr–Cr in line configuration even slightly. This fact enhances the desorption yield during the excitation–deexcitation cycle.

States that have a node in the polar angle θ behave similarly for residence times shorter than 1000 a.u. (24.19 fs). However, for longer residence times, the nodal plane of those states reduces the desorption probability. This part of the wave packet, which corresponds to a region of zero probability density, reaches a position of the electronically excited state where desorption would become efficient after back transfer of the wave packet to the electronic ground state PES. For this reason a saddle point occurs in the course of the desorption probability. This occurrence of saddle points has also been reported and analyzed in previous one-dimensional studies [3,30]. After the nodal plane has passed this critical region, the desorption yield starts to increase again. The behaviour of one state with two nodes in the polar coordinate is also depicted in Fig. 4. Following the previous analysis, two saddle points occur in the desorption probability curve.

The state located in the local minimum first reflects the rovibrational ground state behaviour and then approaches the behaviour of states which are excited within the azimuthal rotation mode.

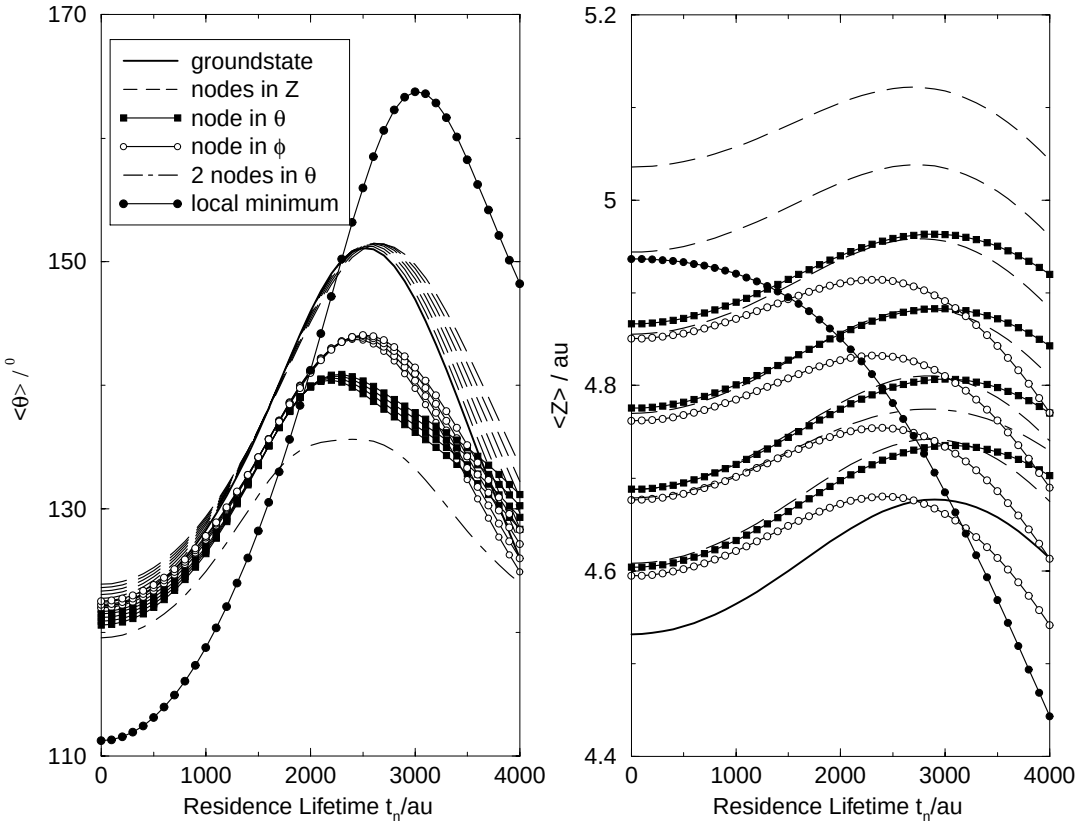

Fig. 3. Expectation values $\langle\theta\rangle$ and $\langle Z\rangle$ for excited state propagation for different eigenstates of the electronic ground state potential (1000 a.u. = 24.19 fs).

4.2. Rotational alignment

The rotational alignment

$$A_0^2(J) = \left\langle J \left| \frac{3M^2 - J^2}{J^2} \right| J \right\rangle$$

of the desorbing CO molecules resulting for the $T = 0$ K limiting case was discussed previously [3,4]. In Fig. 5(left), we show the consequences of selective excitation of several eigenstates on the quadrupole moment A_0^2. All results are lifetime averaged with respect to a resonance lifetime $\tau = 10$ fs. Again, one can observe a strong dependence of the quadrupole moment A_0^2 on the rotational preexcitation. States which are excited in the azimuthal rotational mode yield significant higher helicopter character of the desorbate as compared to the rovibrational ground state and the states which are preexcited in the molecule–surface vibrational mode. This means that the initial 'helicopter excitation' survives the excitation–deexcitation cycles within the DIET process. At low J, the simulated rotational alignment is in better agreement with the experimental data points (shown in the right panel) for these rotationally preexcited states.

States with nodes in the polar angle show the opposite trend: They yield lower helicopter character than the rovibrational ground state. This can be understood as well, since nodes in the polar angle θ favour cartwheel excitation.

While the state with two nodes in the polar angle reflects the rovibrational ground state behaviour, the state which is located in the local minimum does not show any helicopter motion at all. Our explanation of this feature is based on arguments presented previously [3,4]: Helicopter

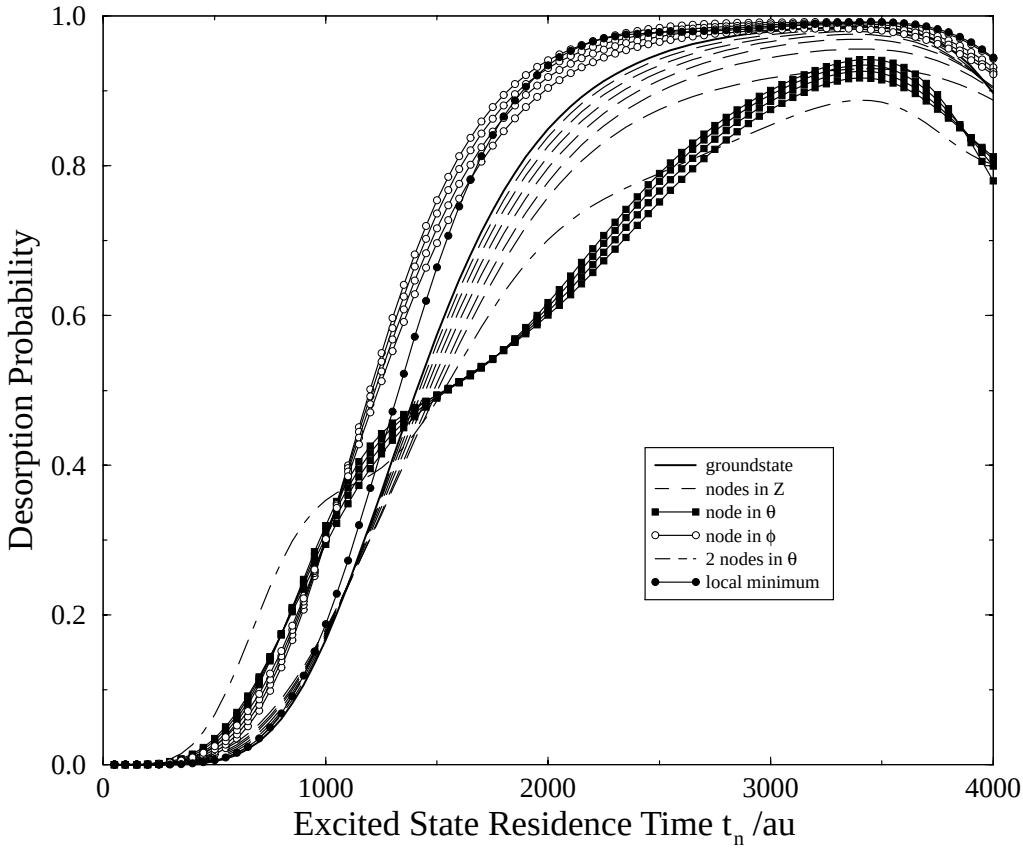

Fig. 4. Desorption probability as a function of the excited state residence lifetime t_n for different initial states.

motion of the desorbate was traced back to an interplay between the opposite directed ϕ-gradients in the electronic ground and excited state. The mechanistic picture was set up as a two step sequence: First, the CO-molecule is forced out of its inline adsorption geometry with respect to the Cr–Cr-axis of the surface by the azimuthal gradient of the excited state PES. After relaxation to the electronic ground state the CO molecule experiences an opposite ϕ-gradient which accelerates the twisted molecule towards its equilibrium geometry, thus exciting helicopter motion. Fig. 6 (straight line) reveals this mechanism when considering the effects of laser irradiation as a sudden vertical transition of the ground state wave packet (located at $\phi = 180°$) to the electronically excited state. Due to its larger equilibrium molecule–surface distance the state located in the local minimum experiences less ϕ-corrugation in both electronic states than the state located in the global minimum. This is also illustrated in Fig. 6 (dashed line). Especially the first step of our mechanism, the helicopter-kick after laser excitation is less pronounced for this state.

For a given rotationally preexcited state vibrational nodes do not shift the quadrupole moment considerably.

5. Influence of temperature

The temperature T is introduced into our quantum mechanical simulations by assuming that the initial states discussed in Section 2 are populated according to a Boltzmann distribution of the level populations. The lifetime averaged quadru-

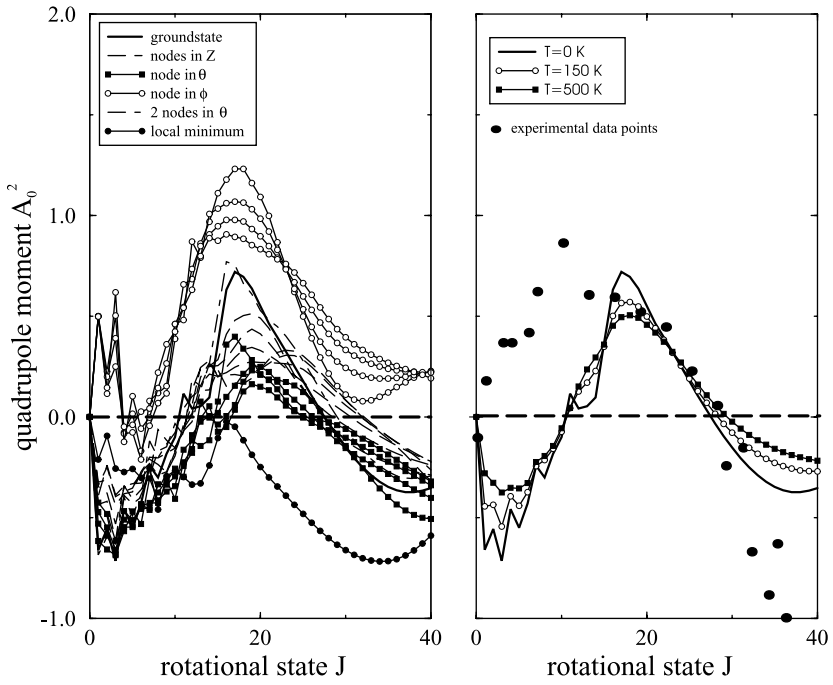

Fig. 5. Left: Quadrupole moment A_0^2 after selective excitation of different eigenstates. Right: Temperature averaged quadrupole moment. All results are lifetime averaged with respect to a resonance lifetime $\tau = 10$ fs.

pole moment $A_0^2(J,i)$ is temperature averaged corresponding to

$$A_0^2(J,T) = \frac{\sum_{i=1}^{N} A_0^2(J,i) \exp\left(-\frac{E_i}{kT}\right)}{\sum_{i=1}^{N} \exp\left(-\frac{E_i}{kT}\right)}. \quad (1)$$

The index i in Eq. (1) corresponds to the separate initial states and k is the Boltzmann constant. To get converged results with respect to Eq. (1), it was sufficient to consider the first $N = 17$ eigenstates of the electronic ground state potential. A temperature interval between 0 and 500 K could then be investigated. The populations given in Table 1 are sufficiently converged for the two chosen exemplary temperatures ($T = 100$ K and $T = 500$ K) with respect to the total number of states. A temperature higher than 160 K is artificial though, since in thermal desorption experiments the CO molecules desorb at about 160 K corresponding to an adsorption energy of 43 kJ/mol [23].

Fig. 5(right) shows the temperature averaged quadrupole moment for $T = 150$ K and $T = 500$ K and the experimental data points. The $T = 0$ K case corresponds to the situation in which only the rovibrational ground state wave packet is propagated within the excitation deexcitation cycle. The influence of temperature on the rotational alignment of the desorbing species is obviously small. The only significant effect of heating up the system in our simulations is that at low J the A_0^2-curve is smoothed when increasing the temperature from 0 to 500 K. In case of the experimental temperature of 100 K, it seems sufficient to consider only the rovibrational ground state wave packet in a sense of a $T = 0$ K limit. The general disagreement between theory and experiment at low J-values has been addressed previously [3,4]. The microscopic reason for the missing temperature effects is based on the low populations of the hindered rotational levels in the relevant temperature regime. At the experimental temperature mainly the molecule–surface bond is excited. Excitation of this vibrational mode has no drastic consequence on the observables of interest as shown in the previous sections. The angular degrees of freedom in prin-

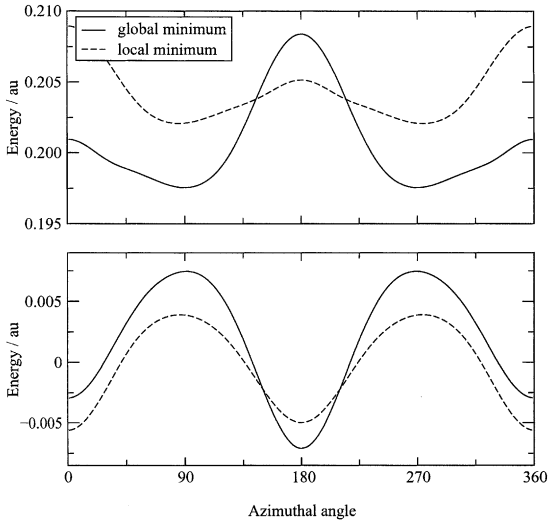

Fig. 6. ϕ-Corrugation of electronic ground state (bottom) and electronically excited state (top). Straight line: situation at $Z = 4.5$ a.u. and $\theta = 122°$ (global minimum). Dashed line: situation at $Z = 4.9$ a.u. and $\theta = 111°$ (local minimum).

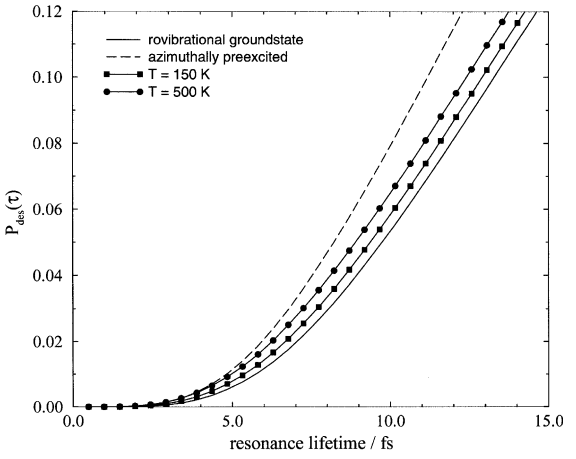

Fig. 7. Lifetime averaged desorption probabilities for different temperatures; the lifetime averaged desorption probability after selective excitation of an azimuthally preexcited state is shown for comparison (dashed line).

ciple account for more pronounced effects than the molecule–surface vibrational mode, but excitation of the hindered rotational modes is simply not efficient in the experimental temperature range. The unphysical $T = 500$ K case in Fig. 5 is useful to show that temperature effects are already close to be at maximum at $T = 100$ K.

In Fig. 7, we show the desorption probability for different surface temperatures. In contrast to Fig. 4, lifetime averaging has been performed in this case. The desorption probability is plotted as a function of the excited state resonance lifetime τ. Temperature enhances the desorption efficiency, but the effects are small. Considering a typical value of 10 fs for the excited state resonance lifetime yields desorption probabilities of 5.3%, 5.8% and 6.5% for $T = 0$ K (rovibrational ground state), $T = 150$ K and $T = 500$ K, respectively. Again, this small effect is due to the fact that at accessible experimental temperatures only the molecule–surface bond is excited. The corresponding eigenstates have less effect on the desorption probability than the hindered rotational levels. This was visible already in Fig. 4, where non-averaged values of P_{des} have been considered. For comparison, in Fig. 7 we show the lifetime averaged desorption probability for a single selected eigenstate, which is azimuthally preexcited. In case of the chosen resonance lifetime of 10 fs, it yields a desorption probability of 8% which is much larger than the result for the rovibrational ground state.

6. Conclusions

The present study can be regarded as a continuation of the simulations presented for the NO/Cr_2O_3(0 0 0 1)-system in one dimension [7]. Inclusion of more degrees of freedom (as the angular coordinates in the present study) yields a detailed picture of the microscopic processes which occur during photodesorption. The hindered rotational levels play only a minor role in a temperature averaging scheme, since they are not significantly populated at the temperatures of interest in the CO/Cr_2O_3(0 0 0 1)-system. At a typical intermediate state resonance lifetime of $\tau = 10$ fs and at the experimental temperature of $T = 100$ K, the small temperature effect on the desorption yield is exclusively due to excitation of the molecule–surface bond. A similar result was achieved for NO/Cr_2O_3(0 0 0 1) with only the molecule–surface coordinate being present [7]. Only at the artificial temperature of $T = 500$ K we observed slight ef-

fects in the low J regime of the quadrupole moment A_0^2. On the other hand, if it was possible to excite separate eigenstates selectively, manipulation of the rotational alignment of the desorbing species would become possible. Of special interest are states with azimuthal preexcitation and the 'flipped' state, which corresponds to occupation of a local minimum of the electronic ground state PES. It is yet to be shown whether these predictions can be checked in experiment.

Acknowledgements

Financial support of this project through the Deutsche Forschungsgemeinschaft (SPP 1093) and the German–Israeli Foundation for Scientific Research and Development (GIF) is greatfully acknowledged. The Centres d'Etudes et de Recherches Lasers et Applications is supported by the Ministère chargé de la Recherche, the Région Nord/Pas de Calais and the Fonds Européen de Développement Economique des Régions.

References

[1] A. Assion, T. Baumert, M. Bergt, T. Brixner, T. Kiefer, V. Seyfried, M. Strehle, G. Gerber, Science 282 (1998) 919.
[2] I. Beauport, K. Al-Shamery, H.-J. Freund, Chem. Phys. Lett. 256 (1996) 641.
[3] S. Thiel, M. Pykavy, T. Klüner, H.-J. Freund, R. Kosloff, V. Staemmler, Phys. Rev. Lett. 87 (2001) 077601.
[4] S. Thiel, M. Pykavy, T. Klüner, H.-J. Freund, R. Kosloff, V. Staemmler, J. Chem. Phys. 116 (2002) 762.
[5] P. Saalfrank, R. Baer, R. Kosloff, Chem. Phys. Lett. 230 (1994) 463.
[6] Q.-S. Xin, X.-Y. Zhu, Chem. Phys. Lett. 265 (1997) 259.
[7] S. Thiel, T. Klüner, M. Wilde, K. Al-Shamery, H.-J. Freund, Chem. Phys. 228 (1998) 185.
[8] P. Saalfrank, S. Holloway, G.R. Darling, J. Chem. Phys. 103 (1995) 6720.
[9] P. Saalfrank, G.K. Paramonov, J. Chem. Phys. 107 (1997) 10723.
[10] G.K. Paramonov, P. Saalfrank, J. Chem. Phys. 110 (1999) 6500.
[11] P. Saalfrank, R. Kosloff, J. Chem. Phys. 105 (1996) 2441.
[12] R.S. Judson, H. Rabitz, Phys. Rev. Lett. 68 (1992) 1500.
[13] W. Zhu, J. Botina, H. Rabitz, J. Chem. Phys. 108 (1998) 1953.
[14] M.D. Feit, J. Fleck Jr., A. Steiger, J. Comput. Phys. 47 (1982) 412.
[15] M.D. Feit, J. Fleck Jr., J. Chem. Phys. 78 (1983) 301.
[16] M.D. Feit, J. Fleck Jr., J. Chem. Phys. 80 (1984) 2578.
[17] R. Kosloff, in: C. Cerjan (Ed.), Numerical Grid Methods and their Application to Schrödinger's Equation, NATO ASI Series, Kluwer Academic Publishers, Dordrecht, 1992.
[18] G.C. Corey, J.W. Tromp, D. Lemoine, in: C. Cerjan (Ed.), Numerical Grid Methods and their Application to Schrödinger's Equation, NATO ASI Series, Kluwer Academic Publishers, Dordrecht, 1992.
[19] D. Lemoine, J. Chem. Phys. 101 (1994) 10526.
[20] G.C. Corey, D. Lemoine, J. Chem. Phys. 97 (1992) 4115.
[21] D. Lemoine, J. Chem. Phys. 101 (1994) 4343.
[22] J.W. Gadzuk, Surf. Sci. 342 (1995) 345.
[23] M. Pykavy, V. Staemmler, O. Seiferth, H.-J. Freund, Surf. Sci. 479 (2001) 11.
[24] M. Pykavy, S. Thiel, T. Klüner, submitted.
[25] R. Kosloff, H. Tal-Ezer, Chem. Phys. Lett. 127 (1986) 223.
[26] P.R. Antoniewicz, Phys. Rev. B 21 (1980) 3811.
[27] D. Menzel, R. Gomer, J. Chem. Phys. 41 (1964) 3311.
[28] P.A. Redhead, Can. J. Phys. 42 (1964) 886.
[29] R. Heather, H. Metiu, J. Chem. Phys. 86 (1987) 5009.
[30] G. Boendgen, P. Saalfrank, J. Phys. Chem. B 102 (1998) 8029.